Nonparametric probabilistic vibroacoustic analysis with Nastran : a computational tool for estimating the likelihood of automobiles experimental FRF measurements

Justin Reyes, Christian Soize, Laurent Gagliardini, Gianluigi Brogna

Nonparametric probabilistic vibroacoustic analysis with Nastran : a computational tool for estimating the likelihood of automobiles experimental FRF measurements

J. Reyes[1,2], **C. Soize**[1], **L. Gagliardini**[2], **G. Brogna**[2,3]
[1] Laboratoire Modélisation et Simulation Multi Echelle, Université Paris Est Marne la Vallée
5 Boulevard Descartes, 77420 Champs-sur-Marne, France

[2] PSA Group, Centre Technique de Vélizy,
Route de Gisy, 78140 Vélizy-Villacoublay, France

[3] Laboratoire Vibrations Acoustique,Université de Lyon
F-69621, Villeurbanne, FRANCE

e-mail: **justin.reyes@mpsa.com, christian.soize@u-pem.fr,**
laurent.gagliardini@mpsa.com, gianluigi.brogna@insa-lyon.fr

Abstract
Improvement of vibroacoustic models prediction capabilities in a probabilistic context requires a adapted metric to compare experimental results with stochasitic computations. The likelihood appears as the natural tool to compare experiments with probabilistic computations as soon as the probability of a given result may be computed. Since vibroacoustic analysis mainly rely on complex Frequency Response Functions ($[\mathrm{FRF}] = \{\omega \mapsto [\mathrm{FRF}(\omega)]\}$) matrices that can be easily measured and computed, the likelihood of such complex and frequency dependent matrices is investigated. A two stage statistical reduction, based on Independant Components Analysis, is proposed in order to separate statisticaly independent components with complex amplitudes which probability may be computed independently one from each others. Bi-dimensional probability density fonctions of the complex components amplitudes are deduced from a Monte-Carlo simulation of a non-parametric stochastic model, using MSC/NASTRAN. The proposed statistical reduction presents many interesting properties regarding the physical understanding of FRF matrices as well as a numerical aspects.

1 Introduction

In the automotive industry, computational vibroacoustic models are used for designing automobiles (see for instance [4, 15, 2]). The acoustic comfort and the vibrations of vehicles is a major issue. In the vibroacoustic analysis, FRFs are widely used to control the structure-borne noise transmission in the case of multiple transmission paths. However, the computational structural model considered in this paper has about fifteen million of degrees-of-freedom (DOFs) and the coupled acoustic cavity has about eight million of DOFs. The high dimension of the computational model brings great difficulties. The advantage of the FRF is that, even for such complex structures such as automobiles, it always provides a simple system of one vector-valued input (excitation) and one vector-valued output (observation). The vibroacoustic computational model allows an easy computation of FRF matrices. The same FRF matrices can also be measured experimentally.

Practical work with FRF requires to handle loadings and observation points. In order to compare experimental measurement with the computational stochastic model results, we propose an approach based on the maximum likelihood method [11, 14], which was introduced in [5, 13]. In this work, we will use the likelihood for quantifying the distance between the experiments and the stochastic computational model. For this purpose, the quantity of most interest is the complex matrix-valued FRF, $[\text{FRF}] = \{\omega \mapsto [\text{FRF}(\omega)]\}$. Both the parameters uncertainties and the model uncertainties induced by the modeling errors are taken into account by the nonparametric probabilistic approach of uncertainties [12, 4, 13, 9]. The principle of this approach consists in replacing the generalized matrices of the reduced-order vibroacoustic computational model by random matrices whose probability distributions are constructed [14] using the maximum entropy principle from Information Theory. Collections of realizations of the FRF matrices can be obtained from a Monte-Carlo simulation. Since Monte-Carlo simulation requires hundreds or thousands of realizations to obtain converged statistics of the results. Consequently, the required storage space may be tremendous.
The proposed approach aims to quantifying the consistency of the stochastic comptational model -described by many of its possible realizations- with the measurements. It is based on two successive statistical reductions that are constructed using Independent Component Analysis (ICA) [7]. These statistical reductions hopefully lead to a high data compression.
In this paper, we will first introduce the nonparametric probabilistic approach of uncertainties together with the FRFs computations. Then, the two statistical reductions will be presented and applied to a computational model of a car. The distance between the predictions and the experiments is then computed using the likelihood concept. Finally, some observations made during this work will be discussed and assessed.

2 Reminder

A computationnal model is constructed by developing a mechanical model of a designed system in order to predict the response of the real system which is a -later- manufactured version of the designed system. The modelling process introduces two kinds of uncertainties : the data uncertainties and the model uncertainties. To achieve some predictivity, these uncertainties have to be taken into account. However, the usual parametric probabilistic approach does not consider the model uncertainties. We will use the nonparametric probabilistic approach of uncertainties Ref.[12] which takes into account both kind of uncertainties. Let us now introduce all the terms that we will use all along this work.
In this approach, the mean values of the generalized matrices of the mass, damping and stifness $[\mathbf{M}]$, $[\mathbf{D}]$ and $[\mathbf{K}]$ are replaced by random matrices $[\mathcal{M}]$, $[\mathcal{D}]$ and $[\mathcal{K}]$. The nonparametric probabilistic approach depends on six hyperparameters controlling the spread of the 3 constitutive matrices of the fluid and structural domains. In this approach the coupling uncertainty is not accounted.
The MSC/Nastran software, in which the nonparametic probabilistic approach has been implemented, is used to produce $n = 1, \cdots, N_{MC}$ samples of an FRF thanks to the Monte Carlo simulation Ref.[10], provided the dispersion hyperparameters δ_A as explained in Ref.[4].

2.1 Nonparametric probabilistic approach

In this paper we consider a linear elastoplastic problem of a complex structure coupled with an internal acoustic cavity. The computational model is constructed using the finite element method (FEM) as shown in Fig.1. The problem is formulated in the frequency domain ω (angular frequency). We are interested in computing FRF of the system in the frequency band analysis noted $\mathbf{B}$ defined by $\mathbf{B} = [\omega_{min}, \omega_{max}]$ with $0 < \omega_{min} < \omega_{max}$ (with $\omega = 2\pi f$). The complex vector $\mathbf{u}(\omega)$ of the m_s degree of freedom (DOF) of the FEM, corresponding to the discretization of the displacements field. Let $\mathbf{p}(\omega)$ the complex vector of the m_f DOFs representing the discretization of the acoustical pressure field. The finite element model is considered

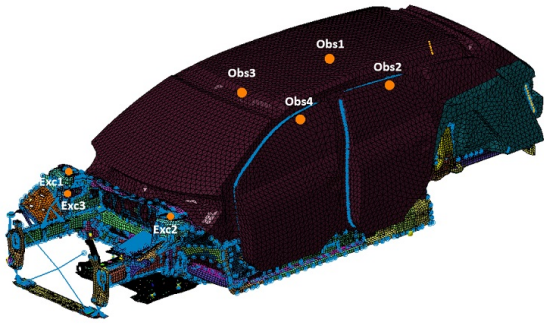

Figure 1: Finite element mesh of the computational model with the excitation and observation points The comptational model has 15 million structural DOFs and 8 million DOFs in the acoustic cavity

as the mean model and is written in the frequency domain as

$$\begin{bmatrix} -\omega^2[M^s] + i\omega[D^s] + [K^s] & [C] \\ \omega^2\,[C]^T & -\omega^2[M^f] + i\omega[D^f] + [K^f] \end{bmatrix} \begin{bmatrix} \mathbf{u}(\omega) \\ \mathbf{p}(\omega) \end{bmatrix} = \begin{bmatrix} \mathbf{f}^s(\omega) \\ \mathbf{f}^f(\omega) \end{bmatrix} \tag{1}$$

Where $[M^s]$, $[D^s]$, and $[K^s]$ are the $(m_s \times m_s)$ positive-defined symmetric real mass matrix, damping and stiffness matrices of the structure where m_s is the number of structural DOFs. And $[M^f]$, $[D^f]$, and $[K^f]$ are the $(m_f \times m_f)$ positive-defined symmetric real mass matrix, damping and stiffness matrices of the structure where m_f is the number of acoustical DOFs. The complex vectors $\mathbf{f}^s(\omega)$ and $\mathbf{f}^f(\omega)$ is related to the discretization of the external forces applied respectively on the structure and in the cavity. $[C]$ the coupling complex matrix between the structure and the acoustic cavity of dimension $(m_s \times m_f)$. For the complex dynamical structures of interest, the number of DOFs can be relatively high. The next step is to construct the nominal ROM which we will consider as the reduced mean computaional model. It is constructed by the usual method of projection on subspace spanned by a set of elastic modes. such that,

$$([K^s] - \lambda^s[M^s])\psi^s = 0 \tag{2}$$
$$([K^f] - \lambda^f[M^f])\phi^s = 0 \tag{3}$$
$$\mathbf{u}(\omega) = [\Psi^s]\mathbf{q}^s(\omega), \tag{4}$$
$$\mathbf{p}(\omega) = [\Phi^f]\mathbf{q}^f(\omega), \tag{5}$$
$$\mathbb{F}^s(\omega) = [\Psi^s]^T\mathbf{f}^s(\omega), \tag{6}$$
$$\mathbb{F}^f(\omega) = [\Phi^f]^T\mathbf{f}^f(\omega), \tag{7}$$
$$[\mathbf{C}] = [\Psi^s]^T[C(\omega)][\Phi^f]. \tag{8}$$

Where $0 < \lambda_1^s \leq \cdots \leq \lambda_{n_s}^s$ are the eigenvalues associated with the eigenvectors $\psi_1^s, \cdots, \psi_{n_s}^s$. The same application is done for λ^f and ϕ^f. $[\Psi^s]$ reprensents the matrix of the eigenvectors such that $[\Psi^s] = [\psi_1^s, \cdots, \psi_{n_s}^s]$ and $[\Phi^f] = [\phi_1^f, \cdots, \phi_{n_f}^f]$. The mean reduced order model is written as

$$\begin{bmatrix} -\omega^2[\mathbf{M}^s] + i\omega[\mathbf{D}^s] + [\mathbf{K}^s] & [\mathbf{C}] \\ \omega^2\,[\mathbf{C}]^T & -\omega^2[\mathbf{M}^f] + i\omega[\mathbf{D}^f] + [\mathbf{K}^f] \end{bmatrix} \begin{bmatrix} \mathbf{q}^s(\omega) \\ \mathbf{q}^f(\omega) \end{bmatrix} = \begin{bmatrix} \mathbb{F}^s(\omega) \\ \mathbb{F}^f(\omega) \end{bmatrix} \tag{9}$$

Then, to take into account the model uncertainties, we use the nonparametric probabilistic aproach of uncertainties , constructed by using the maximum entropy principle. A stochastic ROM is created by replacing the mass, damping and stiffness matrices by random matrices.

$$\begin{bmatrix} -\omega^2[\mathcal{M}^s] + i\omega[\mathcal{D}^s] + [\mathcal{K}^s] & [\mathcal{C}] \\ \omega^2[\mathcal{C}]^T & -\omega^2[\mathcal{M}^f] + i\omega[\mathcal{D}^f] + [\mathcal{K}^f] \end{bmatrix} \begin{bmatrix} \mathbf{Q}^s(\omega) \\ \mathbf{Q}^f(\omega) \end{bmatrix} = \begin{bmatrix} \mathbb{F}^s(\omega) \\ \mathbb{F}^f(\omega) \end{bmatrix} \tag{10}$$

Each random matrix dispersion depends on the hyperparameter $\delta_A > 0$ written as,

$$\delta_A = \sqrt{\frac{E\{|||[\mathbf{G}_A] - [\underline{G}_A]||_F^2\}}{||[\underline{G}_A]||_F^2}}, \tag{11}$$

where $|[\mathbf{G}_A]$ is the random matrix called germ matrix. The construction of the random matrix depends on the random matrix germ as introduced in [13]. This approach has been implemented in Nastran and allow to obtain N_{MC} samples of FRF with the Monte-Carlo method Ref.[10] with values of the dispersion hyperparameter δ_A referenced in [4].

2.2 Frequency response function

For all ω fixed in **B**, (9) has a unique solution

$$\begin{bmatrix}\mathbf{q}^s(\omega)\\ \mathbf{q}^f(\omega)\end{bmatrix} = \underbrace{\begin{bmatrix}-\omega^2[\mathbf{M}^s] + i\omega[\mathbf{D}^s] + [\mathbf{K}^s] & [\mathbf{C}]\\ \omega^2\,[\mathbf{C}]^T & -\omega^2[\mathbf{M}^f] + i\omega[\mathbf{D}^f] + [\mathbf{K}^f]\end{bmatrix}^{-1}}_{[Z]} \begin{bmatrix}\mathbb{F}^s(\omega)\\ \mathbb{F}^f(\omega)\end{bmatrix} \tag{12}$$

The frequency response function of the vibroacoustic system Ref.[9] (that we will work on in this paper) corresponds to the transfer complex matrix such that

$$\mathbf{p}(\omega) = [h(\omega)]\mathbf{f}^s \tag{13}$$

In this paper, we consider $\mathbb{F}^f(\omega) = 0$, then Eq.(12) yields

$$\mathbf{q}^s(\omega) = [Z_{21}]\mathbb{F}^s \tag{14}$$

in which, $[Z_{21}]$ the block matrix of the inverse of the coupling term. From Eqs.(5) and (6), we obtain

$$\mathbf{p}(\omega) = \underbrace{[\Phi^f][Z_{21}][\Psi^s]^T}_{[h(\omega)]}\mathbf{f}^s(\omega) \tag{15}$$

with $[h(\omega)]$ is a complex matrix of dimension $(N_e \times N_o)$. The output of Nastran can be chosen between the displacement, celerity or acceleration field for the structure and the acoustic pressure field for the internal cavity. The output represents directly our FRF by approximation. The principal cause of this appoximation is that the excitations imposed on the system are unitary loadings. FRF gives the representation of a loading (excitation) on a specific location and the reaction it provokes in another place (observation point). And that property is independent of the model complexity.
The finite element model, that we will use is presented in Fig.1. In this study, we will work on the acoustic pressure field of the internal cavity. The observation points (Obs.1-4) represent the listening points of the persons in the vehicle. The structural excitations (Exc.1-3) represent the motor excitations. A vibroacoustic model allow to calculate FRF, which can be measured directly with captors. Those matrices are generally rectangular. Using these matrices, we will propose measure the to predict the likelihood of a measurement in front of the computational model. From now on, the FRF we talked in this paper are either the one computed with Nastran or the experimental measurement.

In Fig.2, we can see the N_{MC} samples of the FRF computed with Nastran and the corresponding experimental measured FRF. It can noticed that the dispersion increase with the frequency. Indeed, it is widely known that the level of uncertainties increases with the frequency. The prediction from numerical simulations are not perfect. There is always a gap between the computational model and experimental measurement. The difference comes from on one hand, the uncertainties of the numerical models and on the other hand from

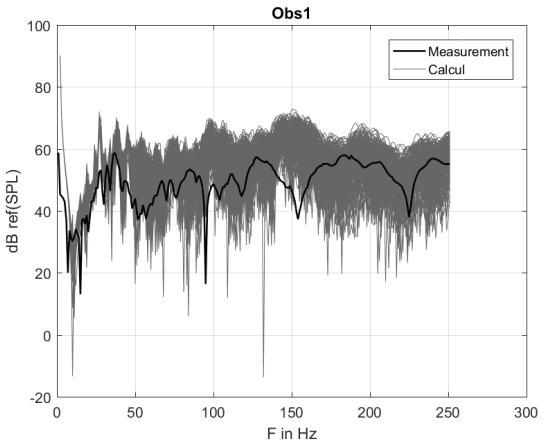

Figure 2: FRF from the nonparametric stochastic approach (grey), FRF from an experimental measurement (black)

the construction of these models. In Fig.2, we can see that in the low-frequency band $[0-20]Hz$, the measurement is very far from the computed FRF. That can be explained partly by the captors. In the next part, we will work on two statistical reductions. The first one will allow to decompose the complex FRF matrix and separate the frequencial component from the spatial component. Then, the second one will permit to decompose the random variable (the N_{MC} samples of Monte-Carlo) from the spatial basis. We know that the Principal Component Analysis (PCA) yields uncorrelated component, and the Independent Component Analysis (ICA) provides independent components. In this paper, we choose the ICA approach with the help of the Joint Approximation Diagonalization of Eigen-matrices (JADE) algorithm.

3 Statistical reductions

In this section, we will propose a two statistical reductions. For that reduction, we will perform the Independent Component Analysis (ICA). The main difference with the Principal Component Analysis (PCA) is that the components will be statistically independent. This approach has been widely used and can be seen in [7]. The ICA can lead to better physical interpretation of the extract components as shown in Fig.3. ICA gives independent components thanks to it's constraint. It should be noted that the PCA and ICA use the same space. The only difference is the constraint imposed on the components which is a linear decorrelation or independency. We use the Joint Approximation Diagonalization of Eigen-matrices (JADE) algorithm as presented in [1] which use the fourth order moments. JADE compute the matrix such as the sum of all non-diagonal term of the fourth order matrix equal to zero. Thus, the matrix is diagonal and proves the independency of the component.
In this paper, it should be noted that $\mathbb{M}_{n,m}(\mathbb{C})$ is the set of all the $(n\times m)$ complex matrices. Let $\omega_1,\cdots,\omega_{N_f}$ be the frequency sampling. Let introduce the observations DOFs noted N_o and the excitations DOFs are called N_e. The FRF complex random matrix written as $[\text{FRF}(\omega_j)]$ with value in $\mathbb{M}_{N_o,N_e}(\mathbb{C})$, with $j=1,\cdots,N_f$. We impose $N=N_o\times N_e$ the spatial dimension. We have $\mathbf{F}(\omega_j)\in\mathbb{C}^N$ the reshape by columns of the complex random matrix $[\text{FRF}(\omega_j)]$. Let $[Y]=[\mathbf{F}(\omega_1),\cdots,\mathbf{F}(\omega_{N_f})]$ with value in $\mathbb{M}_{N,N_f}(\mathbb{C})$. The number of samples noted $n=1,\cdots,N_{MC}$ yields $\{[Y_n],n=1,\cdots,N_{MC}\}$ with N_{MC} independent realizations constructed with the stochastic computational model for a fixed value $\overrightarrow{\mathbf{s}}$ a vector-valued of hyperparameter of the random matrices of the nonparametric approach of uncertainties. For simplifying the writings the dependence on $\overrightarrow{\mathbf{s}}$ is not written.

3.1 First statistical reduction based on ICA

We introduce

$$[R] = \frac{1}{N_{MC}} \sum_{n=1}^{N_{MC}} [Y_n]^*[Y_n] \quad \in \mathbb{M}_{N_f}(\mathbb{C}) \tag{16}$$

in which $[Y_n]^*$ stands for the transpose of the complex conjugated of $[Y_n]$ noted $[\overline{Y}_n]^T$. We resolve the eigenvalue problem of $[R]$ such that $[R]x^\alpha = \lambda_\alpha x^\alpha$, with $\alpha = 1, \cdots, N_f$. This method shows that the eigenvalues λ_α are decreasing. We can approximate $[R]$ with a lower number N_p of terms. Let $N_p \leq N_f$ such that $[R] \simeq \sum_{\alpha=1}^{N_p} \lambda_\alpha x^\alpha (x^\alpha)^*$. The result gives less or equal indepedent principal components than the number of correlated variables. That is rewritten as

$$[R] = [x][\Lambda][x]^*, \tag{17}$$

in which $[\Lambda] \in \mathbb{M}_{N_p}(\mathbb{R})$ and $[x] \in \mathbb{M}_{N_f,N_p}(\mathbb{C})$. $[\Lambda]$ is the diagonal matrix of the eigenvalues such that

$$[\Lambda] = \lambda_\alpha \delta_{\alpha\beta}$$

and $[x] = [x^1, \cdots, x^{N_p}]$ is the matrix of the eigenvectors. It should be noted that

$$[x]^*[x] = [I_{N_p}], \tag{18}$$

It can easily be proven that each realization $[Y_n]$ can be written as

$$[Y_n] = [A_n][x]^* \tag{19}$$

in which, $[A_n] \in \mathbb{M}_{N,N_p}(\mathbb{C})$ is given by the projection on $[Y_n]$. Using Eq.(18),

$$[A_n] = [Y_n][x]. \tag{20}$$

Let

$$[c] = [x]^* \tag{21}$$

be the complex $(N_p \times N_f)$ matrix, for which its columns are denoted by c^j with $j = 1, \cdots, N_f : c = [c^1, \cdots, c^{N_f}]$. Let us introduce the random vector $\overrightarrow{\mathbf{c}}$ with values in $\mathbb{C}^{N_p}$ whose realizations are $c^1, \cdots, c^{N_f}$. We then propose to perform an Indepedent Component Analysis (ICA) of random vector $\overrightarrow{\mathbf{c}}$. We then obtain

$$[c] = [b][S] \tag{22}$$

in which $[b]$ is a $(N_p \times N_p)$ complex matrix and $[S]$ an $(N_p \times N_f)$ complex matrix whose columns noted $S^1, \cdots, S^{N_p}$ are independent. From Eqs.(19), (21),(22), it can be deduced that,

$$[Y_n] = [\widehat{A}_n][S] \tag{23}$$

in which $[\widehat{A}_n]$ is written as

$$[\widehat{A}_n] = [A_n][b] \quad \in \mathbb{M}_{N,N_p}(\mathbb{C}) \tag{24}$$

In this paper, the frequency band analysis noted $\mathcal{B} = [25, 250]Hz$. The frequency basis give N_p independent principle components. The threshold for the cumulative energy is fixed at 95% which is sufficiently high to re-synthesize the FRF by inverse step.

It should be noted that the PCA and ICA use the same space. The only difference is the constraint imposed on the components which is a linear decorrelation or independency. We use the Joint Approximation Diagonalization of Eigen-matrices (JADE) algorithm Ref.[1] which use the fourth order moments. JADE compute

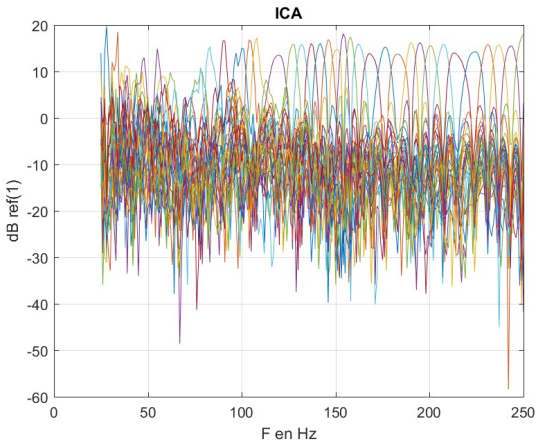

Figure 3: Frequential independent components from JADE algortihm with ICA approach

the matrix such as the sum of all non-diagonal term of the fourth order matrix equal to zero. Thus, the matrix is diagonal and proves the independency of the component. The Fig.3 show the N_p independent components issued from the ICA approach. We can see peaks all along the frequency band **B**. We can suppose that each component has a different contribution over the frequency band. In terms of analysis, we can work on a specific frequency value by working only on the component with the greater contribution over this frequency. We will take the frequency value at the maximum of each independent component from the first ICA statistical reduction from Fig.3. It can be noticed that the contribution of the component is thin in the low frequency. But as the frequency increases, the contribution is widening. By comparing the two approachs, the ICA method which provides an optimal decomposition of the frequency band and a statistically independent component which give us information on the contributions of the components over the frequency band. Now that we have proposed a frequential base with the independent component analysis. In the next part, we will use the same approach to defined a spatial basis. And a stochastic field which will have independent components.

3.2 Second statistical reduction based on ICA

In the second statistical reduction, we will work on the spatial basis over the observations and excitations DOFs. From the N_p independent components from the first statistical reduction over the frequency band, we will determine components with contribution over the spatial basis. We will use exactly the same proposed approach in section 3.1. The independent component analysis is reused for constructing a second statistical reduction of random matrix $[\widehat{A}]$ whose realizations are $\{[\widehat{A}_n], n = 1, \cdots, N_{MC}\}$ defined by Eq.(24). The methodology is exactly the same of the one used in section (3.1) and allows for obtaining the following representation of

$$[\widehat{A}_n]_{k\alpha} = \sum_{\beta=1}^{\widehat{N}_p(\alpha)} [\widehat{F}]_{k\beta}[\chi_n]_{\beta\alpha} \tag{25}$$

with $k = 1, \cdots, N$ and $\alpha = 1, \cdots, N_p$, in which $\widehat{N}_p \leq N$, where $[\widehat{F}(\alpha)]$ and $[\chi_n(\alpha)]$ are complex matrices of dimension $(N \times \widehat{N}_p(\alpha))$ and $(\widehat{N}_p(\alpha) \times 1)$ respectively. $[\chi_n]$ represents the stochastic base over the n

samples of Monte-Carlo, which is our random variable. Substituting Eq.(23) yields

$$[Y_n]_{kj} = \sum_{\alpha=1}^{N_p} \sum_{\beta=1}^{\widehat{N}_p(\alpha)} [\widehat{F}]_{k\beta} [\chi_n]_{\beta\alpha} [S]_{\alpha j} \tag{26}$$

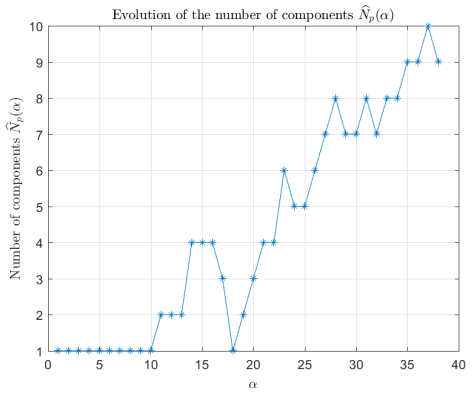

Figure 4: Number of component $\widehat{N}_p(\alpha)$ over the $\alpha = 1, , N_p$ of the first statistical reduction.

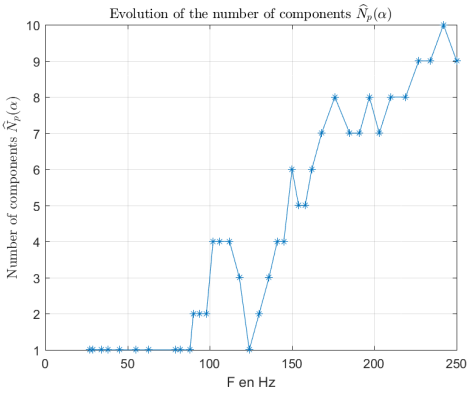

Figure 5: Number of component $\widehat{N}_p(\alpha)$ over the frequency value of the maximum of each α of the first statistical reduction

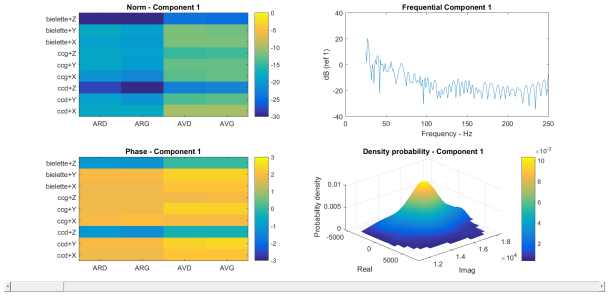

Figure 6: Norm (upper left), phase (bottom left), frequential component (upper right) and the density probability (bottom right) for all γ, here $\gamma = 1$

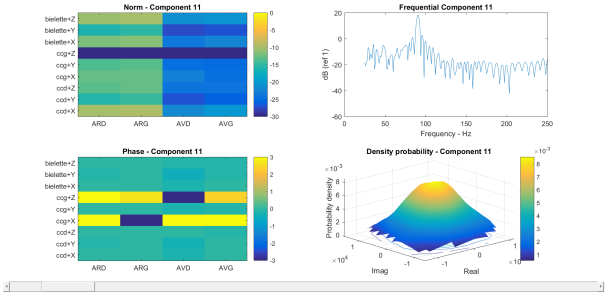

Figure 7: Norm (upper left), phase (bottom left), frequential component (upper right) and the density probability (bottom right) for all γ, here $\gamma = 11$

This statistical reduction is applied to each component from the first statistical reduction. In Fig.4 and 5, it can be noticed that the number of component from the second statistical reduction increases with the frequency. It can be explained by the fact that the model uncertainties increase with the frequency. The Fig.4 and 5 shows that there is an analogy between the value of α and the frequency band. In fact, it can be noticed from Fig.3 that each component of the first statistical reduction has a contribution over a part of the frequency of interest. With this observation we can make an analogy between the value of α and the frequency band. The probability density function of the n samples for each component $\widehat{N}_p(\alpha)$ to create a stochastic basis which will give us the spatial and frequential contribution for each component. The probability density of the component is calculated with the function ksdensity in Matlab. The density probability function is shown in the bottom right in Fig.6 and Fig.7. Moreover, Fig.6 and Fig.7 show the paticipation of each excitation point on each observation point (left figures up and bottom). The upper right figure represents the frequential independent component of the first statistical reduction.

3.3 Projection of the experimental measurement

In this work, we deal with a unique experimental measurement of the same exciation and observation points. We project it on the two-level ROM to obtain χ_{exp}. Note that, for $[Y_n]$ generated with the stochastic implemented in the proposed algorithm yields the values of complex matrices $[S]$, $[\widehat{F}]$ and $[\chi_n]$. For all ℓ = 1, $\cdots$, $\nu_{\exp}$, let $[Y^{\exp}]$ be the $(N \times N_f)$ complex matrix related to given measurements. The corresponding values of $[\chi]$ noted $[\chi^{\exp}]$ are the $(\widehat{N}_p \times N_p)$ complex matrix such that

$$[Y^{\exp,\ell}] = [\widehat{A}^{\exp,\ell}][S] \tag{27}$$

$$[\widehat{A}^{\exp,\ell}]_{k\alpha} = \sum_{\beta=1}^{\widehat{N}_p(\alpha)} [\widehat{F}]_{k\beta}[\chi^{\exp,\ell}]_{\beta\alpha} \tag{28}$$

The projection of Eq.(27) yields

$$[\widehat{A}^{\exp,\ell}] = [Y^{\exp,\ell}][\mathscr{S}] \tag{29}$$

in which $[\mathscr{S}] = [S]^*([S][S]^*)^{-1}$ is the right pseudo-inverse of $[S]$. For α fixed in $\{1, \cdots, N_p\}$, let $[H(\alpha)]$ be the $(\widehat{N}_p(\alpha) \times \widehat{N}_p(\alpha))$ complex matrix defined by

$$[H(\alpha)]_{\beta'\beta} = \sum_{k=1}^{N} [\overline{\widehat{F}}]_{k\beta'}[\widehat{F}]_{k\beta} \tag{30}$$

The projection of Eq.(28) on $[\widehat{F}]$ yields, for α fixed in $\{1, \cdots, N_p\}$ and β' in $\{1, \cdots, \widehat{N}_p(\alpha)\}$, the expression of $[\chi^{\exp,\ell}]$ written as

$$[\chi^{\exp,\ell}]_{\beta'\alpha} = \sum_{k=1}^{N} [\widehat{\mathscr{F}}(\alpha)]_{\beta' k}[\widehat{A}^{\exp,\ell}]_{k\alpha} \tag{31}$$

with $[\widehat{\mathscr{F}}(\alpha)]$ the left pseudo-inverse such that

$$[\widehat{\mathscr{F}}(\alpha)]_{\beta' k} = \sum_{\beta=1}^{\widehat{N}_p(\alpha)} [H(\alpha)^{-1}]_{\beta'\beta}[\widehat{F}]_{k\beta} \tag{32}$$

4 Maximum likelihood method

In this section we will present the maximum likelihood method Ref.[5]. As proposed in Ref.[13], the method consists in introducing a statistic data reduction as done in (section 3.1). Then, to apply the maximum likelihood method to the random variables of the stochastic reduced model. In this study, the random variables are the N_{MC} samples issued from the nonparametric probabilistic approach of uncertainties. χ_n which depends on the component, is the set of random variables from the $n = 1, \cdots, N_{MC}$ realizations. If the number of realization is sufficient, the Kernel smooth density (Ksdensity) Ref.[6] gives a good approximation of the probability density. Let $\widehat{N}_p(\alpha)$ is number of the components of the second statistical reductions for each α. The statistical reduction will be efficient if $\widehat{N}_p(\alpha) << N$. In order to decrease the computational effort, we will work with the two statistical reductions proposed in the section. The ICA approach proposed in this paper offer the advantage of obtaining not only uncorrelated random vectors but furthermore independent components. The family $\{\chi_{\beta\alpha},\ \alpha = 1, \cdots, N_p,\ \beta = 1, \cdots, \widehat{N}_p(\alpha)\}$ of random variables introduced in Eq.(25) are gathered in a random vector $\mathbf{W} = (\mathbf{W}_1, \cdots, \mathbf{W}_{N_{\text{comp}}})$ with $N_{\text{comp}} = \sum_{\alpha=1}^{N_p} \widehat{N}_p(\alpha)$. The corresponding experimental values of $\mathbf{W}$ are denoted by $\{\mathbf{W}^{\exp,\ell}, \ell = 1 \cdots, \nu_{\exp}\}$. Let $(\mathbf{W}_1, \cdots, \mathbf{W}_{N_{\text{comp}}}) \mapsto$

$p(\mathbf{W}_1, \cdots, \mathbf{W}_{N_{\text{comp}}})$ be the probability density function on $\mathbb{R}^{N_{MC} \times \widehat{N}_p(\alpha)}$ (Ref.[13]). We use the following approximation $\mathscr{L}$ of the log-likelihood function of $\mathbf{W}$ for $\gamma = 1, \cdots, N_{\text{comp}}$

$$\mathscr{L} = \sum_{\ell=1}^{\nu_{\text{exp}}} \sum_{\gamma=1}^{N_{\text{comp}}} \mathscr{L}_\gamma \tag{33}$$

with

$$\mathscr{L}_\gamma = 10 \log_{10} p_{\mathbf{W}_\gamma}(\mathbf{W}_\gamma^{\text{exp},\ell}) \tag{34}$$

The probability of an experimental realization from being issued of the stochastic model is given by

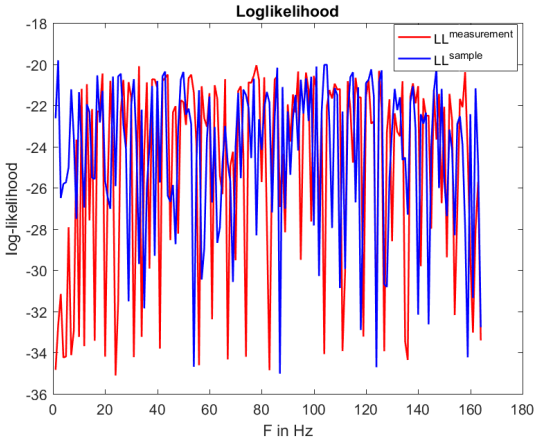

Figure 8: *Loglikelihood* $\mathscr{L}_\gamma$

$$P^{\gamma}_{\mathbf{W}^{\text{exp},\ell}} = p_{\mathbf{W}_\gamma}(\mathbf{W}_\gamma^{\text{exp},\ell}). \tag{35}$$

To be able to visualize the log-likelihood with the components from the first statistical reduction, we rewrite Eq.(33) such that,

$$\mathscr{L} = \sum_{\ell=1}^{\nu_{\text{exp}}} \sum_{\alpha=1}^{N_p} \mathscr{L}_\alpha \tag{36}$$

with

$$\mathscr{L}_\alpha = \sum_{\beta=1}^{\widehat{N}_p(\alpha)} \mathscr{L}_\beta \tag{37}$$

The Fig.9 and 10 shows the maximum and the minimum of the stochastic field. It can be noticed that the sample of Monte Carlo is within the range of the maximum and the minimum. This is an expected result because the stochastic field is made with the n Monte Carlo samples. A verification step has been realized to make sure that all samples are within the range. The experimental measurement is also within the range of the maximum and the minimum. We can interprete it as the model being sufficiently good that the measurement is always between the maximum and the minimum of the computational model. The Fig.10 shows that the experimental measurement is not always in the range of the stochastic field over the N_p component of the first statistical reduction. The interpretation of the loglikelihood over the frequency band comes from the analogy of the components of the first statistical reduction and the frequency at which they are contributing.

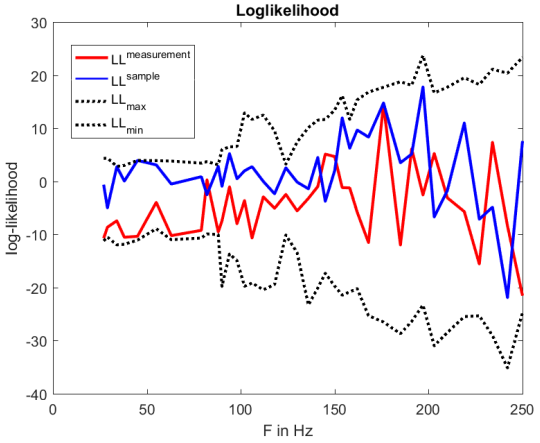

Figure 9: *Log-likelihood of the experimental measurement (red), a sample from Monte Carlo (blue), the minimum and the maximum of the stochastic basis (black dotted)*This example is with dispersion as written in [4]

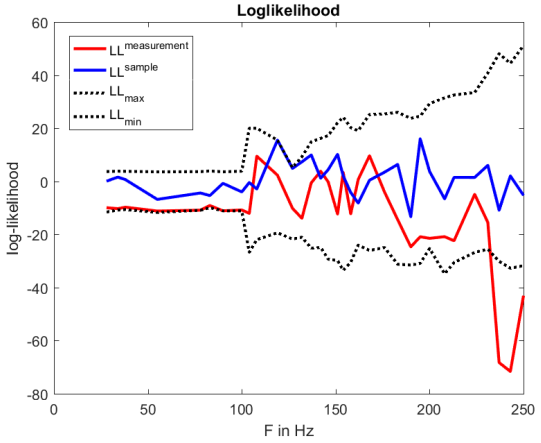

Figure 10: *Log-likelihood of the experimental measurement (red), a sample from Monte Carlo (blue), the minimum and the maximum of the stochastic basis (black dotted)*This example is with low dispersion

5 Additional observations

In this section, we will present some observation made during this work. The first important observation can be used to verify our statistical reductions. By using Eqs.(26) and (23), we will go back to the physical space and resynthesize the FRF. This will allow us to check the threshold we imposed in the eigenvalue problem. With the threshold at 95% as presented in this paper, we compute $[Y_n]$ and compare it with the initial input corresponding FRF.

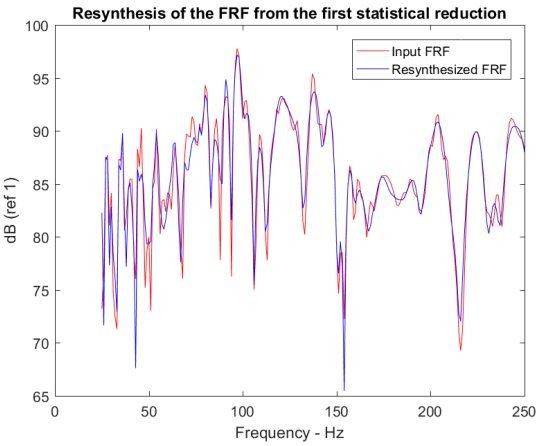

Figure 11: Resynthesized FRF from the first statistical reduction

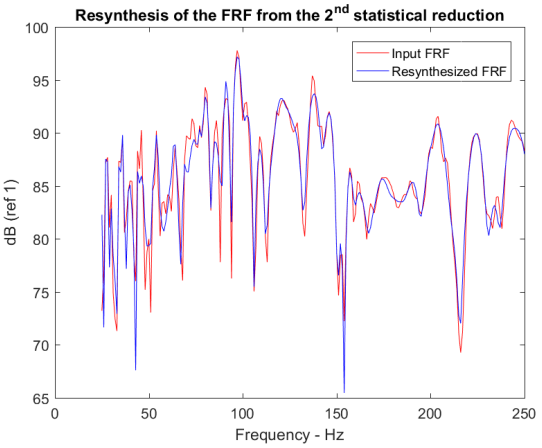

Figure 12: Resynthesized FRF from the second statistical reduction

The Figs.11 and 12 shows the resynthesized FRF with the corresponding input FRF. With the threshold at 95%, we can notice that we effectively have a loss compared to the initial FRF. The slight difference comes from the data reduction. In fact, we keep only 95% of the cumulative energy content for each eigenvector of the input FRF which explain the loss of some data from the initial FRF. Moreover, the resynthesis from the first and the second statistical reduction are identical. This value of the threshold can be considered sufficient for our analysis. The Figs.13 and 14 shows the resynthesized FRF with the corresponding input FRF. With the threshold at 99%, we can notice that the loss is lower and is really close to the input FRF. Moreover, the resynthesis from the first and the second statistical reduction are also identical. This value of

the threshold can be used for this analysis but the computation cost will be greater and the data reduction factor less effective.

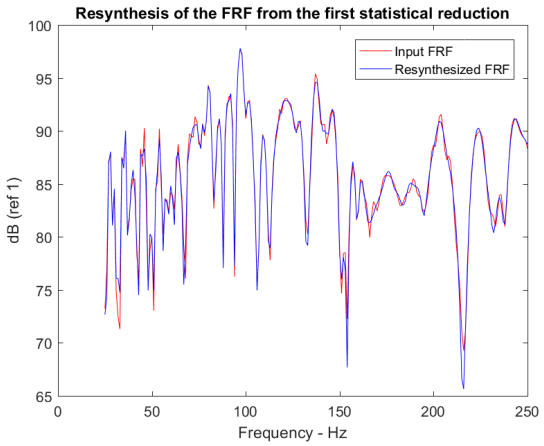

Figure 13: Resynthesized FRF from the first statistical reduction

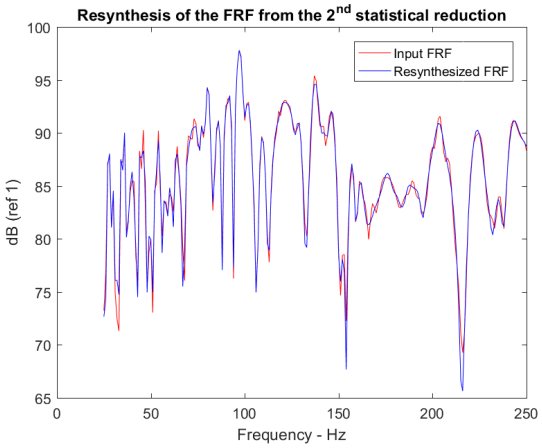

Figure 14: Resynthesized FRF from the second statistical reduction

The data reduction factor noted F_{red} is given by

$$F_{red} = \frac{N \times N_f \times N_{MC}}{N_{\text{comp}} \times (N + N_{MC}) + (N_p \times N_f)} \tag{38}$$

Let τ the threshold of the cumulative energy. The value of F_{red} vary with τ. The Tab.1 shows that the

τ	0.80	0.90	0.95	0.99
F_{red}	78	48	34	20

Table 1: F_{red} in terms of τ

evolution of the statistical data reduction depends on τ. When τ increases F_{red} decreases. The more the dimension of the input data is important, the more the possibility to obtain a great data reduction factor is high.

The last point of the observations is to plot the FRF from the maximum of the probability density function for each component $\gamma = 1, \cdots, N_{\text{comp}}$.
Figs.$15 - 16$ show the FRF issued from the maximum density probability function. The figures shows that for each value of $k = 1, \cdots, N$ the synthesized FRF can be in or out of the N_{MC} input FRF.

6 Conclusion

In this paper, we have presented a methodology for constructing a statistical reduced-order representation of the random matrix-valued FRF that is constructed using a high-dimension stochastic computational model of a car. This reduced representation has been validated by resynthesizing the matrix-valued FRF by an inverse step. This proposed reduction is very efficient in terms of CPU time and RAM. The use of the likelihood method has allowed for estimating the distance between the predictions of the random matrix-valued FRF and the experiments.

In this paper, we will start with a summary of the nonparametric probabilistic approach of uncertainties and a description of the FRF. Then, the two statistical reductions will be presented and will be applied to a computational model of a car with fifteen million of degrees-of-freedom. The FRF will be re-synthesized by inverse step, which will allow for validating the statistical reductions that are proposed. Finally, we will present the distance between the predictions and the experiments using a likelihood method.

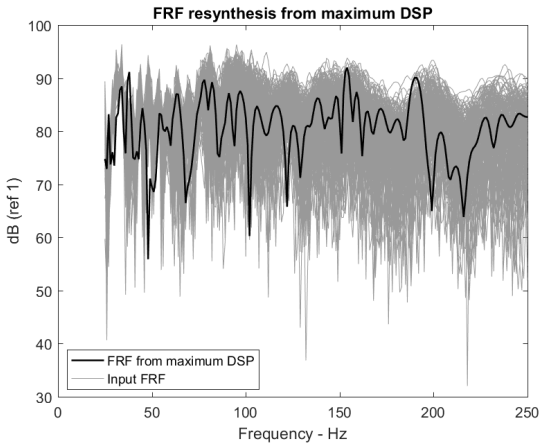

Figure 15: FRF resynthesis from maximum PDF with $k = 1$

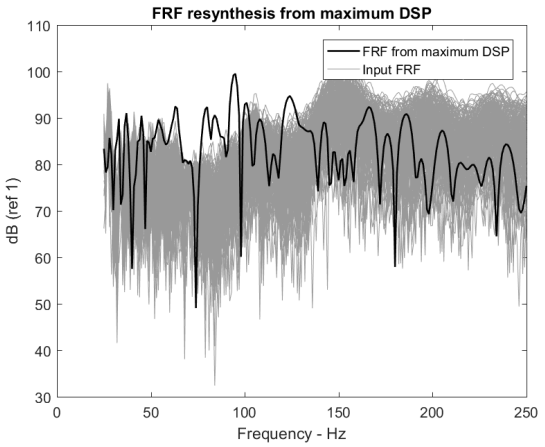

Figure 16: FRF resynthesis from maximum PDF with $k = 26$

References

[1] J.-F. Cardoso, A. Souloumiac, *Blind beamforming for non-Gaussian signals*, IEEE Proceedings F (Radar and Signal Processing), Vol. 140, No. 6 (1993), pp. 362-370.

[2] R. Citarella, L. Federico (eds), *Advances in Vibroacoustics and Aeroacoustics of Aerospace and Automotive Systems*, Applied Sciences, MDPI, Basel, Switzerland (2018).

[3] R. Dony, *et al.*, *Karhunen-Loève transform*, The transform and data compression handbook, Vol. 1 (2001), pp. 1-34.

[4] J.-F. Durand, C. Soize, L. Gagliardini, *Structural-acoustic modeling of automotive vehicles in presence of uncertainties and experimental identification and validation*, Journal of the Acoustical Society of America, Vol. 124, No. 3 (2008), pp. 1513-1525.

[5] C. Fernandez, C. Soize, L. Gagliardini, *Sound-insulation layer modelling in car computational vibroacoustics in the medium-frequency range*, Acta Acustica United with Acustica (AAUWA), Vol. 96, No. 3 (2010), pp. 437-444.

[6] P. D. Hill, *Kernel estimation of a distribution*, Communications in statistics - Theory ad Methods. Vol. 14, No. 3 (1985), pp. 605-620.

[7] A. Hyvarinen, J. Karhunen, E. Oja, *Independant Component Analysis*, John Wiley and Sons, Hoboken, New Jersey (2004).

[8] *MSC Nastran Dynamic Analysis User's Guide*, 2017.

[9] R. Ohayon, C. Soize, *Advanced Computational Vibroacoustics - Reduced-Order Models and Uncertainty Quantification*, Cambridge University Press, New York (2014).

[10] R. Y. Rubinstein, D. P. Kroese, *Simulation and Monte Carlo Method*, Second Edition, John Wiley and Sons, Hoboken, New Jersey (2008).

[11] R. J. Serfling, *Approximation Theorems of Mathematical Statistics*, John Wiley and Sons, Hoboken, New Jersey (1980).

[12] C. Soize, *A Nonparametric model of random uncertainties for reduced matrix models in structural dynamics*, Probabilistic Engineering Mechanics, Vol. 15, No. 3 (2000), pp. 277-299.

[13] C. Soize, E. Capiez-Lernout, J.-F. Durand, C. Fernandez, L. Gagliardini, *Probabilistic model identification of uncertainties in computational models for dynamical systems and experimental validation*, Computer Methods in Applied Mechanics and Engineering, Vol. 198, No. 1 (2008), pp. 150-163.

[14] C. Soize, *Uncertainty Quantification. An Accelerated Course with Advanced Applications in Computational Engineering*, Springer, New York (2017).

[15] E. Yuksel, G. Kamci, I. Basdogan, I. *Vibro-acoustic design optimization study to improve the sound pressure level inside the passenger cabin*, Journal of Vibration and Acoustics, Vol. 134, No. 6 (2012), pp. 061017.